Int. J. Electrochem. Sci., 15 **(2020)** 11070 – 11079, doi: 10.20964/2020.11.74

International Journal of
ELECTROCHEMICAL
SCIENCE
www.electrochemsci.org

Controlled Synthesis of $Zn_3(OH)_2V_2O_7 \cdot 2H_2O$ with 3D micro/nano-structure via electrochemical method

Wenping Jiang[1], *Liheng Zhang*[2,3], *Fanqi Min*[2,3,5], *Yuanyu Sun*[1], *Ying Luo*[3,4], *Liqin Yan*[3,4], *Guoju Dang*[3], *Quansheng Zhang*[1,*], *Jingying Xie*[2,3,4,*]

[1] School of Chemical and Environmental Engineering, Shanghai Institute of Technology, Shanghai 201418, China
[2] School of Chemistry and Chemical Engineering, Harbin Institute of Technology, Harbin 150001, Heilongjiang, China
[3] Shanghai Engineering Center of Power and Energy Storage Battery Systems, Shanghai 200245, China
[4] State Key Laboratory of Space Power-Sources Technology ,Shanghai Institute of Space Power Sources, Shanghai 200245, China
[5] Shanghai Power & Energy Storage Battery System Engineering Tech. Co. Ltd., Shanghai 200240, China
[*]E-mail: zhangquansheng@sit.edu.cn, jyxie@mail.sim.ac.cn

Received: 23 July 2020 / *Accepted:* 11 September 2020 / *Published:* 30 September 2020

$Zn_3(OH)_2V_2O_7 \cdot 2H_2O$ is synthesized by an electrochemical method which gives a 3D micro/nano-hierarchical structures consisting of 2D nanosheets that intercrossed each other by self-assembly. The effects of electrolytic parameters (temperature, time, current density, electrolyte concentration) on the powder morphologies are systematically studied and the resulted powders are characterized with XRD, FT-IR, BET, SEM, TEM, etc. The power structure and particle morphology are governed most by the temperature, where higher temperature will lead to better crystallinity and larger particle sizes. The photocatalytic activities of $Zn_3(OH)_2V_2O_7 \cdot 2H_2O$ prepared at 45℃ shows highest photocatalytic activity for MB under UV light irradiation.

Keywords: Controlled Synthesis, electrochemical method, Zinc pyrovanadate.

1. INTRODUCTION

Recently, zinc vanadate have attracted great attention for its excellent chemistry and physical property [1-9]. As an active precursor of zinc vanadate, $Zn_3(OH)_2V_2O_7 \cdot 2H_2O$) have also been intensive studied [10-12]. The $Zn_3(OH)_2V_2O_7 \cdot 2H_2O$ presented a special layered crystal structure that consists of octahedral Zn-O layer and tetrahedron V-O layers, as shown in Figure 1 [13-15]. In addition, the

channels for holes and electrons conduction exists between the V-O layer, which make it efficient for redox reactions from the teeth outwards zinc pyrovanadate.

Micro/nanostructured $Zn_3(OH)_2V_2O_7{\cdot}2H_2O$ can be used as a good luminescence substrates, electrode and photocatalytic materials for its remarkable stability, high activity, high transmittance of visible light [16-17]. Nowadays, the design and controllable synthesis of micro/nanomaterials with hierarchical structure are regarded as the foundation of development and effective utilization of these high-performance materials. Several methods have been proposed to prepare zinc pyrovanadate, such as liquid-phase, co-precipitation, solid-state reaction, sol-gel and hydrothermal methods. Zinc pyrovanadate is first synthesized by P.Y Zavalij through the hydrothermal method with V_2O_5 as vanadium source [14, 18, 19]. However, V_2O_5 is difficult to control the morphology and purity of products because of its poorly soluble in water. Recently NH_4VO_3 has been adopted as vanadium source to synthesize zinc pyrovanadate with nanobelt and flower-like micro-structures, which show higher photocatalytic activity under UV light conditions [20-21]. Yang prepare zinc pyrovanadate via hydrothermal method and find that the sample obtained from low PH presents higher photocatalytic activity [22-23]. Flower-like $Zn_3(OH)_2V_2O_7{\cdot}2H_2O$ has also been synthesized effectively through a simple liquid phase method as a high-performance anode for lithium-ion batteries, which delivers a remarkable specific capacity of 1287 $mAh{\cdot}g^{-1}$ at 0.2 $A{\cdot}g^{-1}$ after 120 cycles [24].

However, a feasible method of preparing micro/nano-$Zn_3(OH)_2V_2O_7{\cdot}2H_2O$ in a large scale is still missing. Electrochemical method has emerged as a new strategy for efficient powder synthesis with controlled morphology. In our previous work, the metal molybdenum ($MMoO_4$,M=Cu, Ni, Zn, Fe) nanoparticles have been prepared by cationic membrane electrolysis method , which demonstrates its advantage of high purity product, no pollution and suitability for industrial production [25-26].

In this study, we adopt the electrochemical method to synthesize $Zn_3(OH)_2V_2O_7{\cdot}2H_2O$ with 3D micro/nanoflower-like structure at a mild temperature. The influence of electrolytic process parameters (temperature, current density, concentration of electrolyte) on target products have been studied. The photo-physical properties and growth process of flower-like $Zn_3V_2O_7(OH)_2{\cdot}2H_2O$ are also explored.

2. EXPERIMENTAL

2.1. Reagents and materials

All chemicals used in this work were of analytical grade without further purification and purchased from Shanghai Sinopharm Chemical Reagent Co. Ltd. Zinc foil (99.99% purity) was washed with acetone (C_3H_6O) and anhydrous ethanol (CH_3CH_2OH). We used zinc foil as the anode and $NaVO_3$ as the anolyte; DSA as the cathode and dilute hydrochloric acid as the catholyte. The temperatures we used are 25, 45, 60 and 75°C, and the densities are 1, 3, 5 and 7A/dm^2 respectively.

2.2. Synthesis of $Zn3(OH)_2V_2O_7·2H_2O$

The $Zn_3(OH)_2V_2O_7·2H_2O$ (the following is denoted as Zn-V-OH) powders were synthesized by electrochemical method in cation exchange membrane electrolytic cell. 90mL $NaVO_3$ aqueous solution was used as anolyte and 90mL dilute hydrochloric acid (HCl) was the catholyte. The Land was used to control the current density and time. The PolyScience was used to control the electrolyte temperature. A 2cm×5cm of Zinc foil was used as the anode, and the DSA was the cathode. DuPont TM Nafion ® PFSA NRE-212 membrane was used to fabricate the cation exchange membrane electrolysis cell. Temperature, current density and time were controlled as the parameters for electrolysis. All samples obtained in anode compartment were washed with deionized water and dried in air. Zinc pyrovanadate was synthesized by electrolysis with reactions

$$Zn^{2+}\text{-}2e^- \longrightarrow Zn^{2+} \quad (1)$$

$$3Zn^{2+}+2VO^{3-}+4OH^-+H_2O \longrightarrow Zn_3（OH）_2V_2O_7\ 2H_2O \quad (2)$$

2.3. Characterization of materials

The morphology and microstructure of the prepared samples were characterized with scanning electron microscope (SEM, S-3400N, Hitachi), transmission electron microscope (TEM) and high resolution transmission electron microscope (HRTEM) from Tecnai-G2-F30, operated at accelerating voltage of 200 kV. The crystal structure of the as-prepared samples were determined by X-ray diffraction (XRD) in the D8 Advance X-ray diffractometer (German Bruker AXS) equipped with graphite monochromator and Cu target (λ≈0.15408 nm) at scanning rate of $5^{\circ}·min^{-1}$ using accelerating voltage of 40 kV and emission current of 40 mA. Infrared spectroscopy (IR) was finished by the IR Affinity Fourier transform infrared spectrometer (FTIR) (Shimadzu, Japan) over a wavelength range of 4000-400 cm^{-1} with a resolution of 4 cm^{-1} averaging 32 scans and the FTIR spectrum was recorded from KBr pellets. The surface areas of asprepared samples were tested by nitrogen adsorption/desorption analysis with a Quantachrome Instruments (Micromeritics ASAP 2020 HD88). Nitrogen adsorption/desorption isotherms were measured on an asap 2020 analyzer. The specific surface areas recorded at 77K was calculated using the Brunauer-ERmmette-Teller (BET) method and pore size distribution were evaluated using the Barrette-Joynere-Halenda (BJH) model. The optical properties of as-prepared flower-like micro/nanostructure $Zn_3(OH)_2V_2O_7·2H_2O$ were studied by UVevis measurements (UV 3600 spectrophotometer) .

2.4. Photocatalytic property of $Zn_3(OH)_2V_2O_7·2H_2O$

The as-prepared products (0.050g) was dispersed in a 100ml solution of methylene blue (MB) (10mg/L) in darkness for 60 min to establish an adsorption/ desorption equilibrium. Then, the system was illuminated under 300W Xe lamp with constant stirring. At different irradiation time intervals, about 5ml solution of MB was measured by UV-vis spectroscopy.

3. RESULTS AND DISCUSSION

The synthesis processes of flower-like Zn-V-OH is shown in Figure 2 . Pure Zn foil was used as the anode, and the DSA as the cathode, and $NaVO_3$ solution as the anolyte. The Na^+ in the anolyte can move through the cation exchange membrane into the catholyte (HCl) after energization, and the Zn anode dissolved into the anolyte as Zn^{2+}, which combined with VO^{3-}, OH^- and H_2O in the anolyte to form the nuclei of Zn-V-OH. The electric fields will accelerate the migration of electrons and thus the self-assembly growth. The 2D nanosheets were formed on the nuclei. Nanosheets will continue grow on the same nuclei to reduce the surface energy, and eventually form the 3D flower-like micro/nanostructure [27].

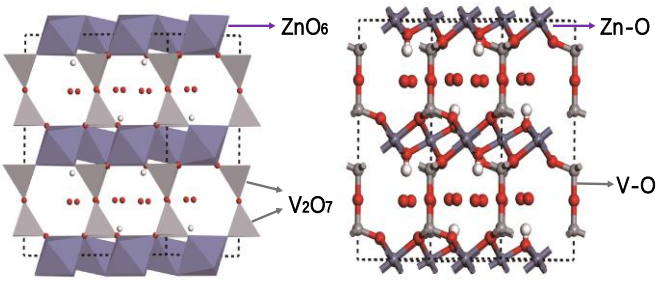

Figure 1. Schematic illustration of the crystal structure of Zn-V-OH

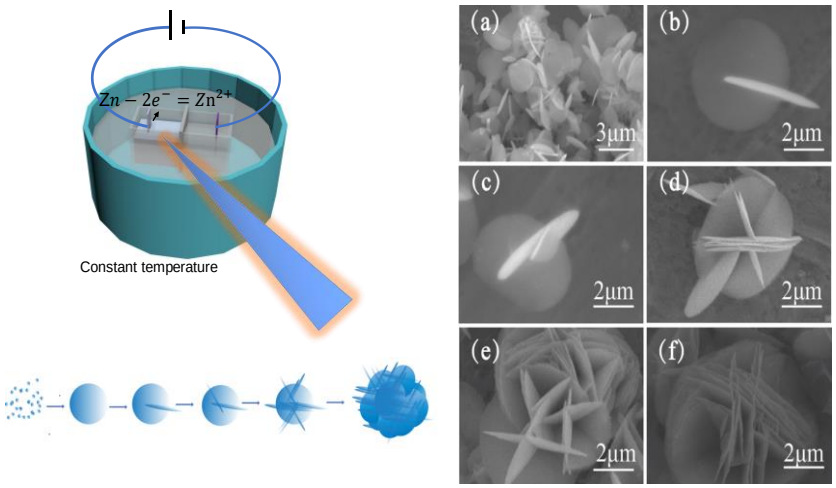

Figure 2. The fabrication processes of flower-like Zn-V-OH

We firstly explored the influence of anolyte concentration on the morphology of products. The experiments were performed in sodium vanadate ($NaVO_3$) with various concentration of 0.1, 0.2, 0.3 and 0.4 $molL^{-1}$, respectively. The current density was controlled at $1A/dm^2$ and the temperature was 75°C. As shown in Figure 3(a)-(d), the flower-like micro/nanostructure consisting of 2D nanosheets are obtained. Agglomeration seems to increase with the concentration. Hence, the lowest concentration of 0.1mol/L was chosen for further experiment.

Subsequently, the electrolyte temperature was fixed at 75℃ but the current density varied at 1, 3, 5 and 7Adm^{-2}. As seen in Figure 3(e)-(h), the final morphologies and sizes are similar to each other. Therefore, the current density seems to only dramatically influence the growth rate.

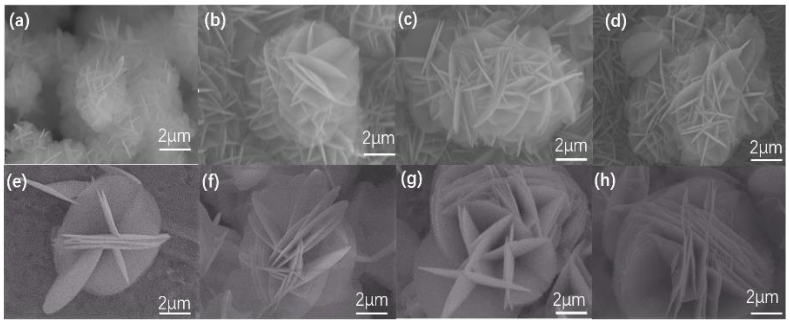

Figure 3. The micrographs of as-prepared products at different electrolyte concentration: (a) 0.1mol/L, (b) 0.2mol/L, (c) 0.3 mol/L, (d) 0.4 mol/L and at different current density: (e)1 A/dm^2, (f) 3 A/dm^2, (g) 5 A/dm^2, (h) 7 A/dm^2.

Finally, the current density was controlled at 1 A dm^{-2}, the electrolyte concentrations was 0.1mol/L, but the electrolyte temperature varied at 25, 45, 60 and 75 ℃. As shown in Figure 3, the particle sizes increase drastically with temperature. The sizes of samples I to IV were 5.5, 3.8, 1.8 and 0.8μm at various temperatures (75 ℃-25 ℃) as listed in Table 1, respectively. The size of the microspheres gradually decreases with the decrease of temperature.

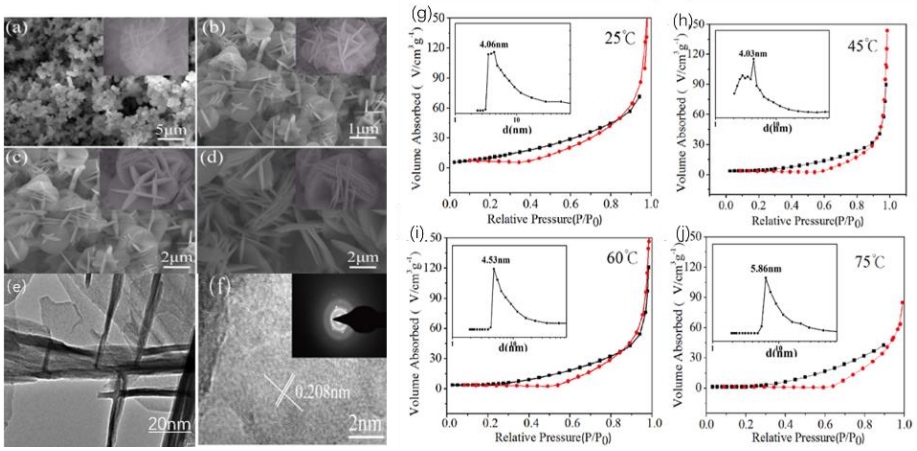

Figure 4. The micrographs of as-prepared products at different temperature: (a) 25℃, (b) 45℃, (c) 60℃, (d) 75℃,(e) TEM at 25℃ (f) HRTEM of samples; Nitrogen adsorption–desorption isotherms and pore size distribution curves of the Zn-V-OH powders prepared at at different temperature. (g) 25℃, (h) 45℃，(i) 60℃, (j) 75℃.

The detailed crystal structure and morphology of hierarchical structures are further investigated by TEM. As shown in Figure 4, plenty of nanosheets fabricated the flower-like structures and

corresponded well with the SEM images. The thicknesses of sheets at different temperature be measured from the TEM and summarized in Table 1. The HRTEM image (Figure 3f) that the lattice fringes of the nanosheet is 0.208 nm, which is consistent with the plane space of (0 2 2). The well aligned diffraction spots in the corresponding SAED patterns indicates that the as-prepared samples exhibits a hexagonal structure.

Table 1. The 3D flower-like Zn-V-OH prepared at different temperature: the sizes and sheet thicknesses

samples	Temperature(℃)	Particle average size (μm)	Sheet thickness(nm)
Zn-V-OH -25	25	0.8	7
Zn-V-OH- 45	45	2.0	12
Zn-V-OH- 60	60	3.8	25
Zn-V-OH- 75	75	5.5	32

The N_2 adsorption–desorption isotherms of the Zn-V-OH powders prepared at different temperature is shown in Figure 4(g)-(j). The isotherm of the samples is of type IV and an evident hysteresis loop is observed, indicating that the pore size distributes within the mesoporous region. [28] The specific surface area of the samples prepared at different temperature are summarized in Table 2. The specific surface areas of sample I to IV are 46.89,23.35,17.12 and11.11m^2g^{-1}, respectively. The pore size distributes mostly within 4-6 nm, which can be attributed to the intraparticle pores in the Zn-V-OH nanosheets [20]. The catalytic reaction usually occur on the surface of catalyst, and a large surface area means more active sites and high catalytic activity. It could be inferred that the sample with smaller size (prepared at a lower temperature) would show higher photocatalytic activity.

Table 2. BET surface area of Zn-V-OH prepared at different temperatures

Sample	Zn-V-OH- 25	Zn-V-OH- 45	Zn-V-OH- 60	Zn-V-OH- 75
BET surface area (m^2/g)	46.89	23.35	17.12	11.11
Mostly probable pore diameter (nm）	4.06	4.03	4..53	5.86

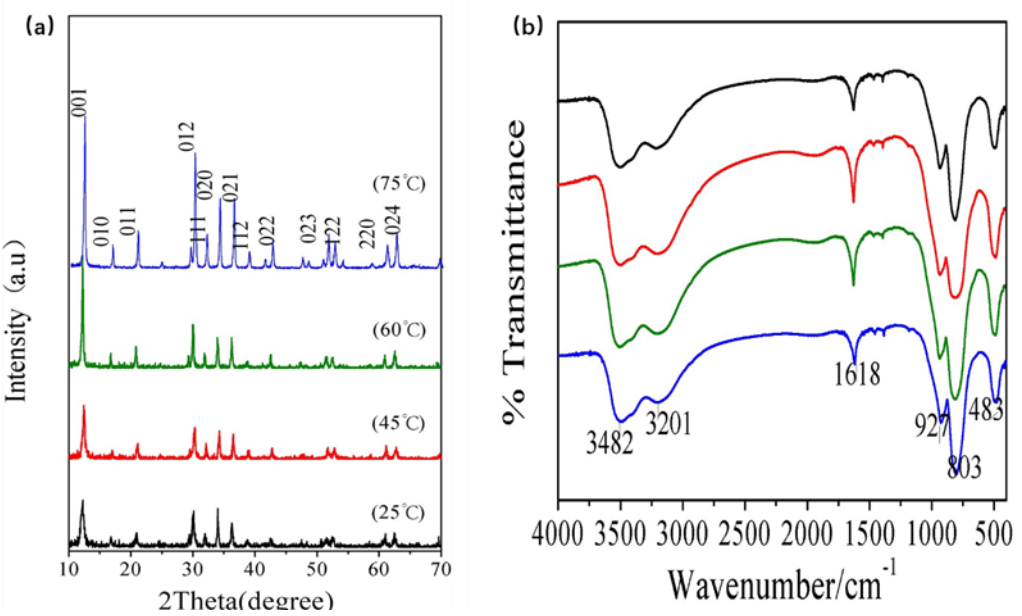

Figure 5. (a)XRD patterns of Zn-V-OH prepared at different temperature;(b) FT-IR spectra of Zn-V-OH prepared at different temperature

The X-ray diffraction peaks of Zn-V-OH synthesized at different temperature in Figure 5a are all pure phase with hexagonal structure (PDF#50-0570). Those diffraction peaks became more sharp with higher intensities, indicating that the samples are better crystallized at higher temperature. The functional groups are further evaluated by Fourier transform infrared (FTIR) spectrum (Figure 4b). All samples illustrate similar FT-IR spectra that the broad absorption peak at 3482 cm^{-1} is the vibration of H-O bonds on the surface of samples, and the weak absorption peak at 1618 cm^{-1} can be assigned to the bending vibration of HO-H bonds.

Several intense absorption peaks in 400–950 cm^{-1} region correspond to symmetric and asymmetric vibrations of M-O-M'. The peaks located at 927 and 483 cm^{-1} should be assigned to V-O-Zn and V-O-V, respectively. The peak at 803 cm^{-1} corresponds to the asymmetric vibrations of V-O-Zn and V-O-V. Obviously, all the bonds corresponding to IR peaks can be referred to Zn-V-OH [18, 28].

The optical properties of Zn-V-OH samples are studied by UV-VIS diffuse reflectance spectroscopy at room temperature. As shown in figure 6a, all the samples depict a strong absorption in the ultraviolet region near the visible-light region, demonstrating its good UV absorption performance in this region [21]. The sample synthesized at 75 ℃ shows slightly different absorption onsets in the UV light region. The absorption onsets of the samples are red-shifted with temperature. Furthermore, the steep shape of the spectra indicated that the absorption is caused by the band-gap transition [29]. The band gap can be estimated with equation

$$\alpha h\nu = K (h\nu - E_g)^{1/n}$$

Where k, α and E_g are constant, the molar extinction coefficient and the average bandgap of the samples separately. Zn-V-OH is a direct gap semiconductor with n=1/2. The optical band energy is calculated by extrapolation of the linear part of plot between the $(h\nu)^2$ vs $(h\nu)$. As shown in Figure 5(c)-(f), the band gap values are 3.53, 3.48, 3.47 and 3.43 eV for samples synthesized at 25, 45, 60, and 75 ℃, respectively.

The photocatalytic activities of Zn-V-OH are evaluated by degradation of MB under UV light irradiation. The results confirms that MB slightly degrades under UV light without catalysts, indicating that the photolysis of MB can be ignored. As shown in Figure 6b, the photocatalytic activities of Zn-V-OH largely depends on the synthesis temperature and particle size. The reaction rate constants k (obtained from first-order linear fitting) of the samples prepared at 25, 45, 60 and 75 ^{o}C are 0.0061, 0.0079, 0.0064 and 0.0049 min^{-1}, respectively. Also, from the value of k, we can conclude that the photocatalytic degradation reaction will occur rapidly on the Zn-V-OH powder prepared at 45℃.

Table 3. illustrates the values of k of Zn-V-OH prepared by different methods

Synthesis method of Zn-V-OH	Reaction rate constant k (min^{-1})	Ref.
template-free hydrothermal route	0.01911	[20]
template-free hydrothermal method.	0.03939	[21]
hydrothermal method	0.1512	[22]
electrochemical method	0.0079	This work

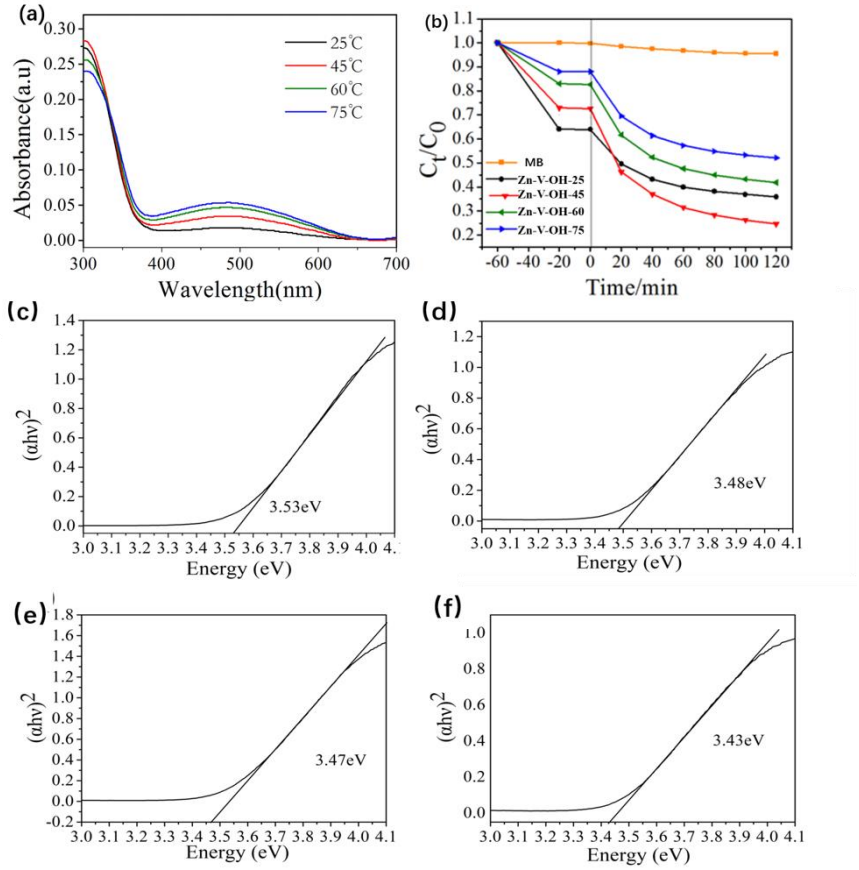

Figure 6. (a)UV-vis spectra of a series of Zn-V-OH; (c-f)Plots of $(h\nu)^2$ vs. hν for the as-prepared Zn-V-OH prepared at different temperatures. (c) 25℃, (d) 45℃, (e) 60℃, (f) 75℃. （b） Photocatalytic degradation curves of samples prepared at different temperatures

Higher synthesis temperature leads to better crystallized powders as observed from previous XRD results, which will decrease amount of lattice defects and thus the photocatalytic activity. Meanwhile, the specific surface area of the samples dramatically decreases with synthesis temperature. These two counter effects of temperature result in an optimized synthesis temperature of 45℃, where a good balance of crystallinity and surface area is obtained.

4. CONCLUSION

Zn-V-OH with 3D flower-like micro/nanostructure are successfully synthesized by electrochemical method at a mild temperature. The influence of electrolytic parameters (temperature, current density, electrolyte concentration) on the morphologies of products have been studied, among which temperature show dominant influences on the structure and sizes of the final products. Higher synthesis temperature will lead to better crystallinity and smaller specific surface area, which have counter effects on the photocatalytic activity. Zn-V-OH prepared at 45℃ shows the highest photocatalytic activity for MB under UV light irradiation. The new synthesis method presented in this work is facile and efficient, which will advances the application of Zn-V-OH as photocatalysts, or even in other electrochemical devices, such as lithium-ion batteries.

AUTHOR CONTRIBUTIONS
W. P. J. and L. H. Z contributed equally.

ACKNOWLEDGEMENT
The author of this article is grateful to the National Natural Science Youth Fund Project (21805186) and the Shanghai Municipal Science and Technology Commission (18DZ2284000, 19DZ2290300) for their strong support.

References

1. M. Zhao, Y. Shi, CS, Tian, *J. Eur. Ceram. Soc*., 31 (2011) 2331.
2. Mrittika Singha, Rajeev Gupta, *J. Phys.: Condens. Matter*, 31 (2019) 495704.
3. Sawsan . Mahmoud· Samar H. Bendary·A. A. Salem·Osama A. Fouad. *SN Appl Sci*., 1 (2019) 497.
4. S. Ezhil Arasi, P. Devendran, R. Ranjithkumar, S. Arunpandiyan, A. Arivarasan. *J. Mater Sci*., 106 (2020) 104785.
5. Lei Luo, Yaqian Fei, Ke Chen, Dawei Li, Xin Wang, Qingqing Wang, Qufu Wei, Hui Qiao. *J. Alloys Compd*., 649 (2015) 1019.
6. Muhammad Munir Sajid, Naveed Akthar Shad, Sadaf Bashir Khan, Zhengjun Zhang, Nasir Amin. *J. Alloys Compd*., 775 (2019) 281.
7. Y.E. Bhoge, V.J. Patil, T.D. Deshpande, R.D. Kulkarni. *Vacuum*, 145 (2017) 290.
8. Khadija Khallouk, Abderrahim Solhy, Abdelhak Kherbeche, Eric Dubreucq, Lamfeddal Kouisni, and Abdellatif Barakat. *ACS Omega*, 5 (2020) 304.
9. Hao Zhu, Lai Ma,Jian Jiang, Zemin Xia, Xi He, Jiao Yang, Baodeng Yang, Qing Li. *Int.J.Electrochem.Sci*.,15 (2020) 371
10. Hangchun Deng, Meiwu Zhu, Tianxiang Jin, Chuanhong Cheng, Jugong Zheng, Yong Qian. *Int.J.*

Electrochem. Sci., 15 (2020) 16
11. Khadija Khallouk, Abderrahim Solhy, Abdelhak Kherbeche, Eric Dubreucq, Lamfeddal Kouisni, and Abdellatif Barakat. *ACS Omega*, 5 (2020) 304.
12. S. Ezhil Arasi, P. Devendran, R. Ranjithkumar, S. Arunpandiyan, A. Arivarasan. *Mater. Sci. Semicond. Process*, 106 (2020) 104785.
13. A. Chowdhury, R. Shukla, V. Sharma, S. Neogy, A. Chandra, V. Grover, A.K. Tyagi. *J. Alloys Compd*., 829 (2020) 154479.
14. S.Y. Zhang, N. Lei, W.Q. Ma, Z.Z. Zhang, Z.B. Sun, Y.J. Wang, *Mater. Lett*., 129 (2014) 91.
15. H.W. Yan, Y.Z. Luo, X. Xu, L. He, J. Tan, Z.H. Li, X.F. Hong, P. He, L.Q. Mai, *ACS Appl. Mater. Interfaces*, 33 (2017) 27707
16. L. Mai, W. Chen, Q. Xu, Q. Zhu, C. Han, J. Peng, *Solid State Commun.*, 126 (2003).
17. X. Chen, X. Sun, Y. Li, *Inorg. Chem*., 41 (2002) 4524.
18. Xiaoyan Han, Qingwen Liu, Wenchuan Song, Haowen Liu. *Solid State Ionics*, 347 (2020) 115250.
19. S. Yang, S. Li, M. Wu, C. Wang, *J. Mater. Chem*., A 4 (2016) 10974.
20. R. Shi, Y. Wang, F. Zhou, Y. Zhu, *J. Mater. Chem*., 21 (2011) 6313.
21. F. Wang, W. Wu, X. Sun, S. Song, Y. Xing, J. Wang, D. Yu, Z, Su, *Mater. Charact*., 86 (2013) 139.
22. S.B. Ni, S.M. Lin, Q.T. Pan, K. Huang, F. Yang, D.Y. He, *J. Alloys Compd*., 477 (2009) L1–L3.
23. G Yang, M Wu, C Wang, *ACS Appl. Mater. Interfaces*, 8 (2016) 23746.
24. H. Yan, Y. Luo, X. Xu, L. He, J. Tan, Z. Li, X. Hong, P. He, L. Mai, *ACS Appl. Mater. Interfaces*, 9 (2017) 27707.
25. J. Yin, F. Min, L. Jia, D. Zhang, Q. Zhang, J. Xie, *J. Mol. Struct*., 1127 (2016) 777.
26. D. Zhang, L. Zhang, W. Zhang, M, Huo, J. Yin, G. Dang, Z. Ren, Q. Zhang, J. Xie, Samuel.S. Mao, *J Mater ionics*, 3 (2017) 135.
27. M. Wang, Y. Shi, G. Jiang, *Mater. Res. Bull.*, 47 (2012) 18.
28. K.S.W. Sing, D.H. Everett, R.A.W. Haul, L. Moscou, R.A. Pierotti, J. Rouquerol, T. Siemieniewska, *Pure Appl. Chem*., 57 (1985) 603.
29. A. Kudo, I. Tsuji, H. Kato, *Chem. Commun.*, 8 (2002) 1958-1959.